

Preconditioned Bi-Conjugate Gradient Method for Radiative Transfer in Spherical Media

L. S. Anusha and K. N. Nagendra

Indian Institute of Astrophysics, Koramangala, Bangalore 560 034, India

and

F. Paletou and L. Léger

Laboratoire d'Astrophysique de Toulouse-Tarbes, Université de Toulouse, CNRS, 14 av. E. Belin, 31400 Toulouse, France.

Received _____; accepted _____

ABSTRACT

A robust numerical method called the Preconditioned Bi-Conjugate Gradient (Pre-BiCG) method is proposed for the solution of radiative transfer equation in spherical geometry. A variant of this method called Stabilized Preconditioned Bi-Conjugate Gradient (Pre-BiCG-STAB) is also presented. These are iterative methods based on the construction of a set of bi-orthogonal vectors. The application of Pre-BiCG method in some benchmark tests show that the method is quite versatile, and can handle hard problems that may arise in astrophysical radiative transfer theory.

Subject headings: Line: formation - radiative transfer - scattering - methods:
numerical

1. Introduction

The solution of transfer equation in spherical geometry remains a classic problem even 75 years after the first attempts by Chandrasekhar (1934); Kosirev (1934), who used Eddington approximation. In later decades more accurate methods were given (see Mihalas 1978; Peraiah 2002, for historical reviews). Hummer & Rybicki (1971), Kunasz & Hummer (1973, 1974) developed a variable Eddington factor method, and computed the solution on rays of constant impact parameter (tangents to the discrete shells and parallel to line of sight) in 1D spherical geometry. This is a very efficient differential equation based technique which uses Feautrier solution along rays of constant impact parameter. An integral equation method was developed by Schmid-Burgk (1974) to solve the problem, again based on tangent rays approach. Peraiah & Grant (1973) presented a highly accurate finite difference method based on the first order form of the transfer equation. All these methods were later extended to expanding, and highly extended atmospheres. However, in this paper we confine our attention to static, 1D spherical atmospheres.

In a next epoch in the development of spherical radiative transfer, the integral operator techniques were proposed. The idea of operator splitting and the use of approximate operators in iterative methods was brought to the astrophysical radiative transfer in planar media by Cannon (1973). Scharmer (1981) extended his work with a new definition of the approximate operator. The application of integral operator technique to the spherical transfer started with the work of Hamann (1985) and Werner & Husfeld (1985). They used approximate operators that are diagonal, constructed from core saturation approach. The $\hat{\Lambda}$ operator contains the non-local coupling between all the spatial points. Olson et al. (1986) showed that the diagonal part (local coupling) of the actual $\hat{\Lambda}$ operator itself is an optimum choice for the ‘approximate operator’. These methods are known as approximate Lambda Iteration (ALI) methods. The ALI methods which are based on the concept of operator

splitting and the use of Jacobi iterative technique, were widely used in the later decades in radiative transfer theory (see Hubeny 2003; Hamann 2003, for historical reviews).

Gros et al. (1997) used an implicit integral method to solve static spherical line transfer problems. The most recent and interesting work on spherical radiative transfer are the papers by Asensio Ramos & Trujillo Bueno (2006) and Daniel & Cernicharo (2008) both of which are based on Gauss-Seidel (GS) and Successive Over Relaxation (SOR) iterative techniques.

Klein et al. (1989) were the first to use BiCG technique in astrophysics. They use BiCG with incomplete LU decomposition technique in their double splitting iterative scheme along with Orthomin acceleration. They applied it to multi-dimensional line transfer problem. Auer (1984) describes a variant of Orthomin acceleration which uses ‘Minimization with respect to a set of Conjugate vectors’. He uses a set of n (usually $n=2$ or $n=4$) conjugate direction vectors which are orthogonal to each other, constructed using the residual vectors with a purpose to accelerate the convergence sequence.

Hubeny & Burrows (2007) developed GMRES (actually its variant called Generalized Conjugate Residuals GCR) method to solve the spherical transfer problem. It is based on an application of the idea of Krylov subspace techniques. They applied it to a more general time-dependent transport with velocity fields in a medium which scatters anisotropically. They apply GMRES method to the neutrino transfer. It can also be used for radiation transfer problem, including the simple problem of 2-level atom line transfer discussed in this paper.

The Preconditioned Bi-Conjugate Gradient method (hereafter Pre-BiCG, see eg., Saad 2000) was first introduced to the line transfer in planar media, by Paletou & Anterrieu (2009) who describe the method and compare it with other prevalent iterative methods, namely GS/SOR. In this paper we adopt the Pre-BiCG method to the case of spherical

media. We also show that the ‘Stabilized Preconditioned Bi-Conjugate Gradient (Pre-BiCG-STAB)’ is even more advantageous in terms of memory requirements but with similar convergence rate as Pre-BiCG method.

It is well known that the spherical radiative transfer in highly extended systems, despite being a straight forward problem, has two inherent numerical difficulties namely (i) peaking of the radiation field towards the radial direction, and (ii) the $(1/r^2)$ dilution of radiation in spherical geometry. To handle these, it becomes essential to take a very large number of angle (μ) points and spatial (τ) points respectively. The existing ALI methods clearly slow down when extreme angular and spatial resolutions are demanded (for example see table 1). Therefore there is a need to look for a method that is as efficient as ALI methods, but faster, and is relatively less sensitive to the grid resolution. The Pre-BiCG method and a variant of it provide such an alternative as we show in this paper.

Governing equations are presented in Sect. 2.1. In Sect. 2.2, we define the geometry of the problem and the specific details of gridding. In Sect. 2.3, the benchmark models are defined. We briefly recall the Jacobi, and GS/SOR methods in Sect. 2.4. In Sect. 3 we describe the Pre-BiCG method. The computing algorithm is presented in Sect. 3.1. In Sect. 4 we describe the Pre-BiCG-STAB method briefly, and we give the computing algorithm in Sect. 4.1. In Sect. 5 we compare the performance of Pre-BiCG with the Jacobi, and GS/SOR methods. In Sect. 6 we validate this new method, by comparing with the existing well known benchmark solutions in spherical line radiative transfer theory. Conclusions are presented in Sect. 7.

2. Radiative transfer in a spherical medium

2.1. The transfer equation

In this paper we restrict ourselves to the case of a 2-level atom model. Further, we assume complete frequency redistribution (CRD). The transfer equation in divergence form is written as

$$\begin{aligned} & \mu \frac{\partial \mathbf{I}(r, \mu, x)}{\partial r} + \frac{1 - \mu^2}{r} \frac{\partial \mathbf{I}(r, \mu, x)}{\partial \mu} \\ & = [\chi_L(r)\phi(x) + \chi_C(r)] \\ & \times [\mathbf{S}(x, r) - \mathbf{I}(r, \mu, x)]. \end{aligned} \quad (1)$$

Here, \mathbf{I} is the specific intensity of radiation, \mathbf{S} - the source function, r - the radial distance, μ - the direction cosine, x - the frequency measured in Doppler width units from line center, $\phi(x)$ - the line profile function, and $\chi_L(r)$, $\chi_C(r)$ - line center and continuum opacities respectively. The differential optical depth element is given by

$$d\tau(r) = -\chi_L(r)dr. \quad (2)$$

There are several methods which use the above form of the transfer equation (see Peraiah 2002). In our paper we solve the transfer equation on a set of rays tangent to the spherical shells. It is written as

$$\begin{aligned} & \pm \frac{\partial \mathbf{I}^\pm(z, p, x)}{\partial z} = [\chi_L(r)\phi(x) + \chi_C(r)] \\ & \times [\mathbf{S}(x, r) - \mathbf{I}^\pm(z, p, x)], \end{aligned} \quad (3)$$

for the outgoing (+) and incoming (-) rays respectively. Here z is the distance along the tangent rays and p is the distance from the center to the points on the vertical axis (the mid-line), where the tangent rays intersect it (see Fig. 1). The direction cosines μ ($0 \leq \mu \leq 1$) are related to p by $\mu = \sqrt{1 - (p^2/r^2)}$ for a shell of radius r . The optical

depth scale along the tangent rays are now computed using $d\tau(z) = d\tau(r)/\mu$. In practical work, due to the symmetry of the problem, it is sufficient to perform the computations on a quadrant only. The source function is defined as

$$\mathbf{S}(x, r) = \frac{\chi_L(r)\phi(x)\mathbf{S}_L(r) + \chi_C(r)\mathbf{S}_c(r)}{\chi_L(r)\phi(x) + \chi_C(r)}. \quad (4)$$

$\mathbf{S}_c(r)$ is the continuum source function taken as the Planck function $\mathbf{B}_\nu(r)$ throughout this paper. The monochromatic optical depth scale $\Delta\tau_x = \Delta\tau_z[\phi(x) + \beta_c]$, with $\beta_c = \chi_C(r)/\chi_L(r)$ along the tangent rays. For simplicity, hereafter we omit the subscript z from τ_z and write τ to denote τ_z . The line source function is given by

$$\begin{aligned} \mathbf{S}_L(r) = (1 - \epsilon) \int_{-1}^1 \frac{d\mu'}{2} \int_{-\infty}^{\infty} dx' \\ \phi(x')\mathbf{I}(\tau, \mu', x') + \epsilon\mathbf{B}_\nu(r), \end{aligned} \quad (5)$$

with the thermalization parameter defined in the conventional manner as $\epsilon = C_{ul}/(A_{ul} + C_{ul})$, where C_{ul} and A_{ul} are collisional and radiative de-excitation rates. The intensity along the rays is computed using the formal solution integral

$$\begin{aligned} \mathbf{I}^+(\tau, p, x) = \mathbf{I}_0^+(\tau, p, x) \exp[-\Delta\tau_x] + \\ \int_{\tau}^T \exp[-\Delta\tau'_x] \mathbf{S}(\tau') [\phi(x) + \beta_c] d\tau'. \end{aligned} \quad (6)$$

The corresponding integral for the incoming rays is

$$\begin{aligned} \mathbf{I}^-(\tau, p, x) = \mathbf{I}_0^-(\tau, p, x) \exp[-\Delta\tau_x] + \\ \int_0^{\tau} \exp[-\Delta\tau'_x] \mathbf{S}(\tau') [\phi(x) + \beta_c] d\tau'. \end{aligned} \quad (7)$$

Here, $\mathbf{I}_0^+(\tau, p, x)$ represents the inner boundary condition imposed at the core and along the mid-vertical line (see Fig. 1). $\mathbf{I}_0^-(\tau, p, x)$ is the outer boundary condition specified at the surface of the spherical atmosphere. When the above formal integral is applied to a stencil of short characteristic (MOP) along a tangent ray, it takes a simple algebraic form

$$\mathbf{I}^\pm(\tau, p, x) = \mathbf{I}_O^\pm(\tau, p, x) \exp[-\Delta\tau_M] +$$

$$\begin{aligned} & \Psi_{\text{M}}^{\pm}(\tau, p, x) \mathbf{S}_{\text{M}} + \Psi_{\text{O}}^{\pm}(\tau, p, x) \mathbf{S}_{\text{O}} + \\ & \Psi_{\text{P}}^{\pm}(\tau, p, x) \mathbf{S}_{\text{P}}, \end{aligned} \quad (8)$$

where $\mathbf{S}_{\text{M,O,P}}$ are the source function values at M, O and P points on a short characteristic. The coefficients Ψ are calculated following the method described in Kunasz & Auer (1988).

2.2. The constant impact parameter approach

In Fig. 1, we show the geometry used for computing the specific intensity $\mathbf{I}(\tau, p, x)$ along rays of constant impact parameter.

In a spherically symmetric medium, we first discretise the radial co-ordinate r ($R_{\text{core}} \leq r \leq R$), where R_{core} is the core radius, and R is the outer radius of the atmosphere. The radial grid is given by $r_k, k = 1, 2, \dots, N_d$, where r_1 is the radius of the outer most shell, and r_{N_d} is that of the inner most shell. $d\Omega/4\pi$ is the probability that the direction of propagation of an emitted photon lies within an element of solid angle $d\Omega$. In the azimuthally symmetric case, it is $d\mu/2$. To calculate the mean intensity $\bar{\mathbf{J}}$ in plane parallel geometry, we integrate the intensity over the angular variable μ itself. In spherical medium, we have one to one correspondence between the (μ, r) and the (p, r) system. In (p, r) system, the probability that a photon is emitted with its impact parameter between p and $p+dp$, propagating in either positive μ or negative μ direction is $pdp/2r\sqrt{r^2 - p^2}$. The direction cosines made by the rays in the (μ, r) space, with a tangent ray of constant p value, are given by $\mu_i = \sqrt{1 - (p^2/r_i^2)}$ at different radii r_i . Therefore the angular integration factor $d\mu/2$ can be changed to $pdp/2r\sqrt{r^2 - p^2}$ (see Kunasz & Hummer 1973).

The p - grid construction: If N_c is the number of core rays, then the p -grid for the core rays is computed using:

$$\text{do } i = 1, N_c$$

$$\begin{aligned}
 p(i) &= R_{\text{core}} * \left(\sqrt{1 - (i/N_c)^2} \right) \\
 0 &< p < R_{\text{core}} \\
 &\text{end do}
 \end{aligned}$$

The number of lobe rays equals the number of radial points. For lobe rays, the p -grid is same as radial r -grid. It is constructed using:

$$\begin{aligned}
 &\text{do } i = 1, N_d \\
 &p(N_c + i) = r(i) \\
 &\text{end do}
 \end{aligned}$$

where N_d =the number of radial points. Thus, the total number of impact parameters is $N_p = N_c + N_d$. We have followed Auer (1984) in defining the p -grid in this manner.

2.3. Benchmark models

Geometrical distances along the rays of constant impact parameter are constructed as follows:

$$z(p, r) = \sqrt{r^2 - p^2}. \quad (9)$$

For spherical shells we perform several tests using power-law type variation of density. For such atmospheres, the line and continuum opacities also vary as a power law given by

$$\chi_{L,C}(r) \propto r^{-\tilde{n}}. \quad (10)$$

Let C and \bar{C} denote the proportionality constants for $\chi_L(r)$ and $\chi_C(r)$ respectively. The constant C can be determined using the optical depth at line center T . For a power law with index \tilde{n} ,

$$C = \frac{T(1 - \tilde{n})}{R^{(1-\tilde{n})} - R_{\text{core}}^{(1-\tilde{n})}}. \quad (11)$$

Using the given input value of $\beta_c = \bar{C}/C$ we can compute the constant \bar{C} .

We use Voigt profile with damping parameter a or the Doppler profile for the results presented in this paper. The spherical shell atmosphere is characterized by the following parameters: $(R, \tilde{n}, T, a, \epsilon, \beta_c, B_\nu)$. We recall that R is the outer radius of the spherical atmosphere surrounding a hollow central cavity of radius R_{core} . When $R = R_{\text{core}}$ we recover the plane parallel limit. For the spherical shell atmospheres, we take $R_{\text{core}} = 1$ as the unit of length to express the radial co-ordinate. The boundary conditions are specified at the outer boundary ($\mathbf{I}^-(\tau = 0, p, x) = 0$) and the inner boundary. There are two types of inner boundary conditions:

(a) *Emitting Core:*

Core rays:

$$\mathbf{I}^+(\tau = T, p \leq R_{\text{core}}, x) = B_\nu. \quad (12)$$

Lobe rays:

$$\mathbf{I}^+(\tau = T, p = r_i, x) = \mathbf{I}^-(\tau = T, p = r_i, x), \quad (13)$$

$i = 1, 2, \dots, N_d$ along the mid-vertical.

(b) *Hollow Core:*

For both the core and the lobe rays:

$$\mathbf{I}^+(\tau = T, p, x) = \mathbf{I}^-(\tau = T, p, x). \quad (14)$$

The hollow core boundary condition is also called ‘planetary nebula boundary condition’ (see Mihalas 1978). It is clear that a spherical shell with a hollow core is equivalent to a plane parallel slab of optical thickness $2T$ with symmetry about the mid-plane at $\tau = T$. We use spherical shell atmospheres for most of our studies.

2.4. Iterative methods of ALI type for a spherical medium

The ALI methods have been successfully used for the solution of transfer equation in spherical shell atmospheres (see eg., Hamann 2003, and references therein). These authors use the Jacobi iterative methods (first introduced by Olson et al. (1986)) for computing the source function corrections. Recently the GS method has been proposed to solve the same problem (see eg., Asensio Ramos & Trujillo Bueno 2006; Daniel & Cernicharo 2008). Hubeny & Burrows (2007) proposed the GMRES method for solving spherical radiative transfer problem. GMRES and Pre-BiCG both belong to Krylov subspace technique. In this paper we compute the spherical transfer solutions by Jacobi and GS/SOR methods, and compare with the solutions computed using the Pre-BiCG method. For the sake of clarity, we recall briefly the steps of Jacobi and GS/SOR methods.

Jacobi Iteration Cycle: The source function corrections are given by

$$\delta \mathbf{S}_k^n = \mathbf{S}_k^{n+1} - \mathbf{S}_k^n = \frac{(1 - \epsilon) \bar{\mathbf{J}}_k^n + \epsilon \mathbf{B}_\nu - \mathbf{S}_k^n}{[1 - (1 - \epsilon) \hat{\Lambda}_{k,k}^*]}, \quad (15)$$

for the n th iterate. Here k is the depth index. The $\hat{\Lambda}^*$ is the approximate operator which is simply taken as the diagonal of the actual $\hat{\Lambda}$ operator defined through

$$\hat{\Lambda}[\mathbf{S}] = \bar{\mathbf{J}}; \quad (16)$$

$$\bar{\mathbf{J}}(\tau) = \int_{-1}^{+1} \frac{d\mu'}{2} \int_{-\infty}^{\infty} dx' \phi(x') \mathbf{I}(\tau, \mu', x'). \quad (17)$$

GS/SOR Iteration Cycle: The essential difference between the Jacobi and GS/SOR methods is the following:

$$\mathbf{S}_k^{n+1} = \mathbf{S}_k^n + \omega \delta \mathbf{S}_k^n. \quad (18)$$

Here the parameter ω is called the relaxation parameter which is unity for the GS technique.

The SOR method is derived from the GS method by simply taking $1 < \omega < 2$ (see Trujillo Bueno & Fabiani Bendicho 1995, for details). The source function correction for the GS method is given by

$$\delta \mathbf{S}_k^n = \frac{(1 - \epsilon) \bar{\mathbf{J}}_k^{n(old+new)} + \epsilon \mathbf{B}_\nu - \mathbf{S}_k^n}{[1 - (1 - \epsilon) \hat{\Lambda}_{k,k}^*]}, \quad (19)$$

where the quantity $\bar{\mathbf{J}}_k^{n(old+new)}$ denotes the mean intensity computed using new values of the source function as soon as they become available. For those depth points for which the source function correction is not yet complete, GS method uses the values of the source function corresponding to the previous iteration (see Trujillo Bueno & Fabiani Bendicho 1995). For clarity we explain how the GS algorithm works in spherical geometry, on rays of constant impact parameter.

Begin loop over iterations

Begin loop over radial shells with index k

Begin loop over impact parameters (or directions) with increasing p

For the n th iteration:

For the incoming rays ($\mu < 0$):

(Reverse sweep along radial shells)

(a) This part of the calculations start at the outer boundary for all impact parameter rays.

(b) \mathbf{I}_k are first calculated for a given radial shell k using \mathbf{S}_k^n , \mathbf{S}_{k-1}^n and \mathbf{S}_{k+1}^n .

(c) The partial integral $\bar{\mathbf{J}}_k(\mu < 0)$ are calculated before proceeding to the next shell. This

part of the calculations is stopped when the core (for the core rays) and the mid-vertical line (for the lobe rays) are reached.

For outgoing rays ($\mu > 0$):
(Forward sweep along radial shells)

(d) This part of the calculations start at the inner boundary. First, for the radial shell with $k = N_d$

$\bar{\mathbf{J}}_{N_d}$ is calculated, using boundary conditions \mathbf{I}_{N_d} .

(e) $\delta\mathbf{S}_{N_d}^n$ is computed and the source function is updated using $\mathbf{S}_{N_d}^{n+1} = \mathbf{S}_{N_d}^n + \delta\mathbf{S}_{N_d}^n$.

(f) For the next radial shell $k = N_d - 1$:

to calculate \mathbf{I}_{N_d-1} by applying the short characteristic formula, \mathbf{S}_{N_d} , \mathbf{S}_{N_d-1} and \mathbf{S}_{N_d-2} are needed. Already $\mathbf{S}_{N_d}^{n+1}$, $\mathbf{S}_{N_d-1}^n$ and $\mathbf{S}_{N_d-2}^n$ are available. GS takes advantage of the available new source function at $k = N_d$. \mathbf{I}_{N_d-1} is calculated with this set of source functions.

(g) Then $\bar{\mathbf{J}}_{N_d-1}(\mu > 0)$ are calculated using \mathbf{I}_{N_d-1} .

(h) Note that, $\bar{\mathbf{J}}_{N_d-1}(\mu < 0)$ was calculated using $\mathbf{S}_{N_d}^n$, $\mathbf{S}_{N_d-1}^n$, and $\mathbf{S}_{N_d-2}^n$ whereas $\bar{\mathbf{J}}_{N_d-1}(\mu > 0)$ used the “updated” source function $\mathbf{S}_{N_d}^{n+1}$. Therefore $\bar{\mathbf{J}}_{N_d-1}$ is corrected by adding the following correction:

$$\Delta\bar{\mathbf{J}}_{N_d-1} = \delta\mathbf{S}_{N_d}^n \int_{-1}^0 \Psi_{N_d}(\mu < 0) d\mu.$$

(i) $\delta\mathbf{S}_{N_d-1}^n$ and $\mathbf{S}_{N_d-1}^{n+1} = \mathbf{S}_{N_d-1}^n + \delta\mathbf{S}_{N_d-1}^n$ are now calculated.

(j) Since “updated” $\mathbf{S}_{N_d-1}^{n+1}$ at $k = N_d - 1$ is also available now, before going to the next radial shell it is appropriate to correct the intensity at the present radial shell by adding to it, the following correction term

$$\Delta \mathbf{I}_{N_d-1}(\mu) = \delta \mathbf{S}_{N_d-1}^n \Psi_{N_d-1}.$$

End loop over impact parameters (or directions)

End loop over radial shells

End loop over iterations.

3. Preconditioned BiCG method for a spherical medium

In this section we first describe the essential ideas of the Pre-BiCG method. The complete theory of the method is described in Saad (2000). We recall that the 2-level atom source function with a background continuum is given by

$$\mathbf{S}(x, r) = \frac{\chi_L(r)\phi(x)\mathbf{S}_L(r) + \chi_C(r)\mathbf{S}_c(r)}{\chi_L(r)\phi(x) + \chi_C(r)}. \quad (20)$$

It can be re-written as

$$\mathbf{S}(x, r) = \tilde{p}(x, r)\mathbf{S}_L(r) + (1 - \tilde{p}(x, r))\mathbf{S}_c(r), \quad (21)$$

where

$$\tilde{p}(x, r) = \frac{\chi_L(r)\phi(x)}{\chi_L(r)\phi(x) + \chi_C(r)}. \quad (22)$$

From equations (5), (16) and (17), we get

$$\begin{aligned} \mathbf{S}(x, r) &= \tilde{p}(x, r)\{(1 - \epsilon)\hat{\Lambda}[\mathbf{S}(x, r)] + \epsilon\mathbf{B}_\nu(r)\} + \\ &(1 - \tilde{p}(x, r))\mathbf{S}_c(r). \end{aligned} \quad (23)$$

Therefore the system of equations to be solved becomes

$$\begin{aligned} [\hat{I} - (1 - \epsilon)\tilde{p}(x, r)\hat{\Lambda}]\mathbf{S}(x, r) &= \tilde{p}(x, r)\epsilon\mathbf{B}_\nu(r) + \\ (1 - \tilde{p}(x, r))\mathbf{S}_c(r), \end{aligned} \quad (24)$$

which can be expressed in a symbolic form as

$$\begin{aligned} \hat{A}\mathbf{y} &= \mathbf{b}; \quad \text{with} \\ \hat{A} &= [\hat{I} - (1 - \epsilon)\tilde{p}(x, r)\hat{\Lambda}]; \quad \mathbf{y} = \mathbf{S}(x, r). \end{aligned} \quad (25)$$

The vector \mathbf{b} represents quantities on the RHS of equation (24). Now we describe briefly, how the Pre-BiCG method differs from ALI based methods.

Let \mathbb{R}^n denote the n -dimensional Euclidean space of real numbers.

Definition: The Pre-BiCG algorithm is a process involving projections onto the m -dimensional subspace ($m \leq n$) of \mathbb{R}^n

$$\mathcal{K}_m = \text{span}\{\mathbf{v}_1, \hat{A}\mathbf{v}_1, \dots, \hat{A}^{m-1}\mathbf{v}_1\}, \quad (26)$$

and also being orthogonal to another m -dimensional subspace of \mathbb{R}^n

$$\mathcal{L}_m = \text{span}\{\mathbf{w}_1, \hat{A}^T\mathbf{w}_1, \dots, \hat{A}^{T(m-1)}\mathbf{w}_1\}. \quad (27)$$

Here \mathbf{v}_1 is taken as the initial residual vector $\mathbf{r}_0 = \mathbf{b} - \hat{A}\mathbf{y}_0$ with \mathbf{y}_0 the initial guess for the solution of equation (25). The vector \mathbf{w}_1 is taken as arbitrary such that the inner product $\langle \mathbf{v}_1, \mathbf{w}_1 \rangle \neq 0$. The method recursively constructs a pair of bi-orthogonal bases $\{\mathbf{v}_i; i = 1, 2, \dots, m\}$ and $\{\mathbf{w}_i; i = 1, 2, \dots, m\}$ for \mathcal{K}_m and \mathcal{L}_m respectively, such that they satisfy the bi-orthogonality condition $\langle \mathbf{v}_i, \mathbf{w}_j \rangle = \delta_{ij}$. For the purpose of application to the radiative transfer theory it is convenient to write the Pre-BiCG steps in the form of an algorithm. For simplicity we drop the explicit dependence on variables.

3.1. The Preconditioned BiCG Algorithm

Our goal is to solve equation (25). In this section the symbols \mathbf{r}_i and \mathbf{p}_i are used to be in conformity with the standard notation of residual and conjugate direction vectors. They should not be confused with the radius vector r_i and impact parameter p_i which appear in spherical radiative transfer theory.

(a) The very first step is to construct and store the matrix \hat{A}^T (which does not change with iterations, for the cases considered here, namely 2-level atom model). Details of computing \hat{A}^T efficiently is described in appendix A.

We follow the preconditioned version of the BiCG method. Preconditioning is a process in which the original system of equations is transformed into a new system, which has faster rate of convergence. For example, this can be done by solving the new system $\hat{M}^{-1}\hat{A}\mathbf{y} = \hat{M}^{-1}\mathbf{b}$ where \hat{M} is an appropriately chosen matrix, called the “preconditioner” (See also equation 2 of Auer 1984). This preconditioner is chosen in such a way that,

- (i) the new system should be easier to solve,
- (ii) \hat{M}^{-1} itself should be inexpensive to operate on an arbitrary vector,
- (iii) the preconditioning is expected to increase the convergence rate.

The choice of the preconditioner depends on the problem at hand. When an appropriate $\hat{\Lambda}^*$ is chosen such that the amplification matrix $[\hat{I} - (1 - \epsilon)\hat{\Lambda}^*]$ has as small a maximum eigenvalue as possible (see Olson et al. 1986), the convergence rate is enhanced. What enables the convergence of ALI, that satisfies the above property, and simplest to manipulate, is the diagonal of the $\hat{\Lambda}$ itself. Therefore the amplification matrix $[\hat{I} - (1 - \epsilon)\hat{\Lambda}^*]$ with a diagonal form for $\hat{\Lambda}^*$ is a simple and natural choice as a ‘preconditioner’. We construct the preconditioner matrix \hat{M} by taking it as the diagonal of \hat{A} .

(b) An initial guess for the source function is

$$\mathbf{y}_0 = \tilde{p}\epsilon\mathbf{B} + (1 - \tilde{p})\mathbf{S}_c, \quad (28)$$

where the thermal part $\epsilon\mathbf{B}$ is taken as an initial guess for \mathbf{S}_L .

(c) The formal solver is used with \mathbf{y}_0 as input to calculate $\bar{\mathbf{J}}(\mathbf{y}_0)$.

(d) The initial residual vector is computed using

$$\mathbf{r}_0 = \mathbf{b} - \hat{A}\mathbf{y}_0. \quad (29)$$

(e) The initial bi-orthogonal counterpart \mathbf{r}_0^* for \mathbf{r}_0 is chosen such that we have $\langle \mathbf{r}_0, \mathbf{r}_0^* \rangle \neq 0$. One can choose $\mathbf{r}_0^* = \mathbf{r}_0$ itself.

Such an initial choice of \mathbf{r}_0^* vector is necessary, as the method is based on the construction of bi-orthogonal residual vectors \mathbf{r}_i and \mathbf{r}_i^* recursively, for $i = 1, 2, \dots, m$, where m is the number of iterations required for convergence. The process of constructing the bi-orthogonal vectors gets completed, once we reach the convergence. In other words, the number of bi-orthogonal vectors necessary to guarantee a converged solution represents the actual number of iterations itself. It is useful to remember that when we refer to ‘bi-orthogonality’ hereafter, say eg., of the residual vectors $\mathbf{r}_i, \mathbf{r}_i^*$ we simply mean that $\langle \mathbf{r}_i, \mathbf{r}_j^* \rangle = 0$ for $i \neq j$, but $\langle \mathbf{r}_i, \mathbf{r}_i^* \rangle$ need not be unity.

(f) The bi-orthogonalization process makes use of conjugate direction vectors \mathbf{p} and \mathbf{p}^* for each iteration. They can be constructed during the iterative process, again through recursive relations. An initial guess to these vectors is made as $\mathbf{p}_0 = \mathbf{r}_0$ and $\mathbf{p}_0^* = \mathbf{r}_0^*$.

(g) The preconditioned initial residual vectors ζ_0^* are computed using

$$\zeta_0^* = \hat{M}^{-1} \mathbf{r}_0^*. \quad (30)$$

(h) For $i = 1, 2, \dots$, the following steps are carried out until convergence:

(i) Using the formal solver with \mathbf{p}_i as input (instead of actual source vector \mathbf{y}), $\bar{\mathbf{J}}[\mathbf{p}_i]$ is obtained.

(j) $\hat{A}[\mathbf{p}_i]$ is computed using

$$\hat{A}[\mathbf{p}_i] = \mathbf{p}_i - (1 - \epsilon) \tilde{p} \bar{\mathbf{J}}[\mathbf{p}_i]. \quad (31)$$

(k) The inner products

$$\langle \hat{A}[\mathbf{p}_i], \mathbf{p}_i^* \rangle \quad \text{and} \quad \langle \mathbf{r}_i, \zeta_i^* \rangle, \quad (32)$$

are computed and used to estimate the quantity

$$\alpha_i = \frac{\langle \mathbf{r}_i, \zeta_i^* \rangle}{\langle \hat{A}[\mathbf{p}_i], \mathbf{p}_i^* \rangle}. \quad (33)$$

(l) The new source function is obtained through

$$\mathbf{y}_{i+1} = \mathbf{y}_i + \alpha_i \mathbf{p}_i. \quad (34)$$

Test for Convergence: Let $\bar{\omega}$ denote the convergence criteria. If

$$\max_{\tau} \{ \delta \mathbf{y} / \mathbf{y} \} \leq \bar{\omega}, \quad (35)$$

then iteration sequence is terminated. Otherwise it is continued from step (m) onwards.

The convergence criteria $\bar{\omega}$ is chosen depending on the problem.

(m) Following recursive relations are used to compute the new set of vectors to be used in the $(i + 1)$ th iteration:

$$\mathbf{r}_{i+1} = \mathbf{r}_i - \alpha_i \hat{A}[\mathbf{p}_i], \quad (36)$$

$$\mathbf{r}_{i+1}^* = \mathbf{r}_i^* - \alpha_i \hat{A}^T[\mathbf{p}_i^*], \quad (37)$$

$$\zeta_{i+1}^* = \hat{M}^{-1} \mathbf{r}_{i+1}^*. \quad (38)$$

(n) The quantity β_i is computed using

$$\beta_i = \frac{\langle \mathbf{r}_{i+1}, \zeta_{i+1}^* \rangle}{\langle \mathbf{r}_i, \zeta_i^* \rangle}. \quad (39)$$

(o) The conjugate direction vectors for the $(i + 1)$ th iteration are computed through

$$\begin{aligned} \mathbf{p}_{i+1} &= \mathbf{r}_{i+1} + \beta_i \mathbf{p}_i, \\ \mathbf{p}_{i+1}^* &= \mathbf{r}_{i+1}^* + \beta_i \mathbf{p}_i^*. \end{aligned} \quad (40)$$

(p) The control is transferred to step (g).

The converged source function \mathbf{y} is finally used to compute the specific intensity everywhere within the spherical medium.

4. Transpose free variant - Pre-BiCG-STAB

In spite of higher convergence rate, computation and storage of the \hat{A}^T matrix is a main dis-advantage of the Pre-BiCG method. To avoid this, and to make use of only the ‘action’ of \hat{A} matrix on an arbitrary vector, a method called ‘BiCG-squared’ was developed (See Saad 2000, for references and details), which is based on squaring the residual polynomials. Later it was improved by re-defining the residual polynomial as a product of two polynomials and obtaining a recursive relation for the new residual polynomial. This

product involves residual polynomial of the Pre-BiCG method and a new polynomial which ‘smoothens’ the iterative process. In this section we give the computing algorithm of the Pre-BiCG-STAB method as applied to a radiative transfer problem. As described below, we can avoid computing and storing of the \hat{A}^T matrix in the Pre-BiCG-STAB method. However we would now need to call the formal solver twice per iteration unlike in Pre-BiCG method, where it is called only once. This results in an increase in number of operations per iteration when compared to Pre-BiCG method, causing a slight increase in the CPU time per iteration. In spite of these the Pre-BiCG-STAB method turns out to be always faster than the regular Pre-BiCG method in terms of convergence rate (lesser number of iterations for convergence).

4.1. Pre-BiCG-STAB algorithm

Now we give the algorithm of Pre-BiCG-STAB method to solve the system $\hat{M}^{-1}\hat{A}\mathbf{S} = \hat{M}^{-1}\mathbf{b}$. Here \hat{M} is a suitably chosen preconditioner matrix. The computing algorithm is organized as follows:

(a) First initial preconditioned residual vectors and conjugate direction vectors are defined through

$$\mathbf{z}_0 = \hat{M}^{-1}\mathbf{b} - \hat{M}^{-1}\hat{A}\mathbf{S}, \quad (41)$$

$$\mathbf{z}_0^* = \mathbf{z}_0, \quad \mathbf{P}_0 = \mathbf{z}_0. \quad (42)$$

(b) For $j = 1, 2, \dots$ the following steps are carried out until convergence.

(c) Using \mathbf{P}_j instead of the source function a call to the formal solver is made to compute $\hat{A}\mathbf{P}_j$.

(d) The coefficient α_j can be evaluated now as

$$\alpha_j = \frac{\langle \mathbf{z}_j, \mathbf{z}_0^* \rangle}{\langle \hat{M}^{-1} \hat{A} \mathbf{P}_j, \mathbf{z}_0^* \rangle}. \quad (43)$$

(e) Another vector \mathbf{q}_j is calculated as

$$\mathbf{q}_j = \mathbf{z}_j - \alpha_j \hat{M}^{-1} \hat{A} \mathbf{P}_j. \quad (44)$$

(f) Using \mathbf{q}_j in place of the source function a call to the formal solver is made to obtain $\hat{A} \mathbf{q}_j$.

(g) The coefficient ω_j is estimated as

$$\omega_j = \frac{\langle \hat{M}^{-1} \hat{A} \mathbf{q}_j, \mathbf{q}_j \rangle}{\langle \hat{M}^{-1} \hat{A} \mathbf{q}_j, \hat{M}^{-1} \hat{A} \mathbf{q}_j \rangle}. \quad (45)$$

(h) The updated new source function is calculated as

$$\mathbf{S}_{j+1} = \mathbf{S}_j + \alpha_j \mathbf{P}_j + \omega_j \mathbf{q}_j. \quad (46)$$

(i) Test for convergence is made as in the Pre-BiCG algorithm.

(j) Before going to the next iteration a set of recursive relations are used to compute residual vectors

$$\mathbf{z}_{j+1} = \mathbf{q}_j - \omega_j \hat{M}^{-1} \hat{A} \mathbf{q}_j, \quad (47)$$

and conjugate direction vectors

$$\mathbf{P}_{j+1} = \mathbf{z}_{j+1} + \beta_j (\mathbf{P}_j - \omega_j \hat{M}^{-1} \hat{A} \mathbf{P}_j). \quad (48)$$

for the next iteration, where the coefficient β_j is

$$\beta_j = \frac{\langle \mathbf{z}_{j+1}, \mathbf{z}_0^* \rangle \alpha_j}{\langle \mathbf{z}_j, \mathbf{z}_0^* \rangle \omega_j}, \quad (49)$$

(k) The control is now transferred to the step (b).

5. Comparison of ALI and Pre-BiCG methods

There are two characteristic quantities that define iterative techniques. They are (a) convergence rate, which is nothing but the maximum relative change (MRC) defined as

$$R_c = \max_{\tau} \left\{ \frac{\delta \mathbf{S}^n}{\mathbf{S}^n} \right\}, \quad (50)$$

and (b) the total CPU time T_{total} required for convergence. T_{total} is the time taken to reach a given level of convergence, taking account only of the arithmetic manipulations within the iteration cycle. We also define a quantity called the true error T_e and use it to evaluate these methods.

5.1. The behaviour of the maximum relative change (MRC)

In this section we compare R_c and T_{total} for the Jacobi, GS, SOR, Pre-BiCG and the Pre-BiCG-STAB methods. The SOR parameter used is 1.5. It is worth noting that the overrates (the time taken to prepare the necessary set up, before initiating the iterative cycle) are expected to be different for different methods. For instance, in Jacobi and GS/SOR this is essentially the CPU time required to set up the $\hat{\Lambda}^*$ matrix. In the Pre-BiCG method this involves the time taken to construct the \hat{A}^T matrix, which is a critical quantity of this method. The Pre-BiCG method is described in this paper in the context of a 2-level atom model, because of which, we do not need to update the \hat{A}^T matrix at each iteration.

For the Pre-BiCG-STAB method it is the time taken to construct the preconditioner matrix \hat{M} .

Fig. 2 shows a plot of R_c for different methods. We can take R_c as a measure of the convergence rate. Chevallier et al. (2003) show that it always becomes necessary to use high resolution grids, to achieve high accuracy of the solution (See also Sect. 1 of this paper). This is especially true in the case of spherical radiative transfer where a spatial grid with a large number of points per decade becomes necessary to achieve reasonable accuracy. In the following we discuss how different methods respond to the grid refinement. It is a well known fact with the ALI methods, that the convergence rate is small when the resolution of the depth grid is very high. In contrast they have a high convergence rate in low resolution grids. On the other hand the R_c of Pre-BiCG and Pre-BiCG-STAB methods have higher convergence rate even in a high resolution grid. Fig. 2(a) shows R_c for different methods when a low resolution spatial grid is used (5pts/D in the logarithmic scale for τ grid). The Jacobi method has a low convergence rate. In comparison, GS has a convergence rate which is twice that of Jacobi. SOR has a rate that is even better than that of GS. However Pre-BiCG and the Pre-BiCG-STAB methods have the higher convergence rate. Fig. 2(b) and 2(c) are shown for intermediate (8 pts/D) and high (30 pts/D) grid resolutions. The essential point to note is that, as the grid resolution increases, the convergence rate decreases drastically and monotonically for the Jacobi and the GS methods. It is not so drastic for the SOR method which shows non-monotonic dependence on grid resolution. The Pre-BiCG and Pre-BiCG-STAB methods exhibit again a monotonic behaviour apart from being relatively less sensitive to the grid resolution.

In Table 1 we show what happens when we set convergence criteria to progressively smaller values ($\bar{\omega} = 10^{-6}$, 10^{-8} , and 10^{-10} for Tables 1(a), 1(b) and 1(c) respectively) for various grid resolutions. The model used to compute these results is $(\tilde{n}, R, T, a, \epsilon, \beta_c, B_\nu) =$

$(0, 10, 10^3, 10^{-3}, 10^{-4}, 0, 1)$. The idea is to demonstrate that for a given grid resolution (corresponding rows of the Tables 1(a), 1(b) and 1(c)), all the methods show a monotonic increase in the number of iterations for convergence, as we decrease the $\bar{\omega}$. On the other hand Pre-BiCG and Pre-BiCG-STAB require much less number of iterations to reach the same level of accuracy.

CPU time considerations: Table 2 shows the CPU time requirements for the methods discussed in this paper. The model used to compute these test cases is $(\tilde{n}, R, T, \epsilon, \beta_c, B_\nu, \bar{\omega}) = (0, 300, 10^3, 10^{-4}, 0, 1, 10^{-8})$. The grid resolution considered is 30 pts/D. The CPU time for convergence can be defined as the computing time required to complete the convergence cycle and reach a fixed level of accuracy. We recall that the overrates in computing time is the time taken to prepare the necessary set up before initiating the iterative cycle. Total computing time is the sum of these two. In appendix A we discuss in detail how to construct \hat{A}^* matrix for Jacobi, GS/SOR methods and \hat{A} and \hat{M} matrices for Pre-BiCG and Pre-BiCG-STAB methods respectively with an optimum effort. Construction of these matrices constitutes the overrates in computing time of each method. The first row of Table 2 shows that Pre-BiCG is the fastest to complete the convergence cycle. The reason why Pre-BiCG-STAB takes slightly longer time than Pre-BiCG is explained at the end of Sect. 4.

The second row of Table 2 shows that all methods except Pre-BiCG take nearly 8 seconds as overrates for the chosen model. Pre-BiCG takes additional 3-4 seconds as explicit integrals are performed for computing off-diagonal elements also (Unlike the other methods where such integrals are performed only for diagonal elements).

The last row of Table 2 shows that in terms of total CPU time requirement, the other methods fall behind the Pre-BiCG and the Pre-BiCG-STAB. Pre-BiCG seems to be a bit faster compared to Pre-BiCG-STAB for the particular model chosen. However it is model

dependent. For instance, as the contribution towards overrates increases, Pre-BiCG-STAB clearly stands out as the fastest method of all, discussed in this paper.

5.2. A study of the True Error

We now study the true errors in these methods (see Figure 3). The model parameters are $(\tilde{n}, R, T, \epsilon, \beta_c, B_\nu) = (0, 10, 10^3, 10^{-4}, 0, 1)$. A coherent scattering limit is used. To define a true error, we need a so called ‘exact solution’. Except for highly idealized cases, exact solutions do not exist. For practical purposes, the exact solution can be defined as a solution obtained on a spatial grid of resolution that is three times larger than the grid resolution of the model that we are interested in. Also, we extend the iteration until R_c reaches an extremely small value of 10^{-12} . The source function computed in this way can be called $\mathbf{S}(\infty, \infty)$ (fully converged solution on an infinite resolution) (see Auer et al. 1994). The source function at the n th iterate is denoted by \mathbf{S}^n . We define the true error as

$$T_e = \max_{\tau} \left| \frac{\mathbf{S}^n - \mathbf{S}_{\text{exact}}}{\mathbf{S}_{\text{exact}}} \right|, \quad (51)$$

following Trujillo Bueno & Fabiani Bendicho (1995). In Fig. 3(a) we show T_e computed for the Pre-BiCG method using three grid resolutions, namely 10 pts/D, 14 pts/D and 20 pts/D. The plateau of each curve represents the minimum value of the true error reached for a given grid resolution. We notice that as the resolution increases, T_e gradually decreases in magnitude as expected. In Fig. 3(b) we show T_e computed for the Pre-BiCG-STAB method. The model parameters are same as in Fig. 3(a). Clearly, Pre-BiCG-STAB shows a smooth decrement of true error compared to Pre-BiCG, because of the smoothing polynomial used to define the residual vectors. In Fig. 3(c) we compare the decrement of true errors for different iterative methods. The grid resolution chosen is 14 pts/ D with other model parameters being same as in Figs. 3(a), (b). The decrease of the true errors follows the same pattern in all the iterative methods, although the number of iterations required for

T_e to reach a constant value (plateau) depends on the method. To reach the same level of true error, the Pre-BiCG and Pre-BiCG-STAB methods require considerably less number of iterations, when compared to the other three.

5.3. A theoretical upper bound on the number of iterations for convergence in the Pre-BiCG method

Suppose that \hat{A} is an $N_d \times N_d$ matrix. The solution to the problem $\hat{A}\mathbf{y} = \mathbf{b}$ is a vector of length N_d . In an N_d -dimensional vector space V_{N_d} the maximum number of linearly independent vectors is N_d . Hence, there can at the most be N_d orthogonal vectors in V_{N_d} . The Pre-BiCG method seeks a solution by constructing orthogonal vectors. We recall that the residual counterpart vectors $\{\mathbf{r}_1^*, \mathbf{r}_2^*, \dots, \mathbf{r}_M^*\}$ constructed during the iteration process are orthogonal to the initial residual vector \mathbf{r}_0 . Thus, when we reach convergence after M iterations, we will have a set of $M + 1$ orthogonal vectors $\{\mathbf{r}_0, \mathbf{r}_1^*, \mathbf{r}_2^*, \dots, \mathbf{r}_M^*\}$. From the arguments given above, it is clear that $M + 1 \leq N_d$, namely in the Pre-BiCG method, ‘the convergence must be reached theoretically in at the most N_d steps (or iterations)’. This sets an upper limit to the number of iterations to reach convergence (see also Hestenes & Stiefel 1952). For example when the dimensionality of a problem is high (very large value of N_d), the Pre-BiCG method ensures convergence in at the most N_d iterations. A theoretical upper bound on the number of iterations also exists for the Pre-BiCG-STAB method, whereas the other methods do not have such a theoretical upper bound. In practice we find that Pre-BiCG and Pre-BiCG-STAB methods actually require much less number of iterations than N_d , even when N_d is large.

6. Results and discussions

The main purpose of this paper is to propose a new method to solve the line transfer problems in spherically symmetric media. In this section we show some illustrative examples in order to compare with the famous benchmarks for spherical transfer solutions presented in the papers by Kunasz & Hummer (1974). In Fig. 4 we show source functions for different test cases. Fig. 4(a) shows the source functions for $\epsilon = 10^{-2}$ and $\epsilon = 10^{-4}$ for $R = 300$ and $T = 10^3$. Other model parameters are $(\tilde{n}, \beta_c, B_\nu) = (2, 0, 1)$. We use a Doppler profile to compare with the results of Kunasz & Hummer (1974). Plane parallel result is also shown for comparison. When $\epsilon = 10^{-2}$ we observe that the thermalization is reached at the thermalization length for the Doppler profile namely $1/\epsilon = 100$. When $\epsilon = 10^{-4}$ thermalization does not occur. Clearly the minimum value of the source function is ϵB_ν . For the large values of $R = 300$ and opacity index $\tilde{n} = 2$, as r increases the opacity decreases steadily and the source function indeed approaches this minimum value near the surface layers. For this case, the departure of the source function from planar limit is severe near the surface. It can be shown (dashed line of Fig. 4(b), see also Fig. 3 of Kunasz & Hummer (1974)) that this departure is not so acute when $\tilde{n} = 0$, but is more acute when $\tilde{n} = 3$ (dash triple-dotted line in Fig. 4(b)). In Fig. 4(b) we plot source function for the same model as Fig. 4(a) but for various values of \tilde{n} . For negative \tilde{n} , the distinction between $\mathcal{S}(\tau)$ vs. τ curves for different \tilde{n} is small. For positive \tilde{n} , the effects are relatively larger (see dot-dashed and long dashed curves in Fig. 4(b)).

In Fig. 4(c), we show source function variation for a range of spherical extensions R . We have chosen an effectively optically thin model $(T, \epsilon) = (10^8, 10^{-10})$ because in such a medium, thermalization effects do not completely dominate over the effects of sphericity. Other parameters are same as in Fig. 4(b). Clearly, the decrease in the value of source function throughout the atmosphere is monotonic, with an increase in the value of R from

1 to 10^6 .

In Fig. 5, we show effects of limb darkening in spherical atmospheres for $R = 10^3$ and $R = 10^6$. The other model parameters for Fig. 5(a) are $(\tilde{n}, T, \epsilon, \beta_c, B_\nu) = (2, 10^8, 10^{-4}, 0, 1)$. A Doppler line profile is used. From the Figure, we notice absorption in the line core and emission in the near line wings ($x \approx 4$) for $\theta = 0^\circ$ and 10° . This is the characteristic self reversal observed in spectral lines formed in extended spherical atmospheres. The self reversal decreases gradually as θ increases, and finally vanishes for large values of θ . Indeed for extreme value of $\theta = 90^\circ$, we observe a pure emission line.

In Fig. 5(b) we show line profiles formed in a semi-infinite spherical medium. The model parameters are same as in Fig. 5(a) except for $(R, T) = (300, 10^{12})$. The profiles for a range of $\theta = 0^\circ, 31^\circ, 54^\circ, 72^\circ, 84^\circ$ are shown. For the core rays ($\theta = 0^\circ$) we see a pure absorption line due to thermalization of source function. For other angles, as expected we see chromospheric type self-reversed emission lines, formed in the lobe part of the spherical medium.

7. Conclusions

In this paper we propose a robust method called Preconditioned Bi-Conjugate Gradient (Pre-BiCG) method to solve the classical problem of line transfer in spherical media. This method belongs to a class of iterative methods based on the projection techniques. We briefly present the method, and the computing algorithm. We also present a transpose-free variant called the Stabilized Preconditioned Bi-Conjugate Gradient (Pre-BiCG-STAB) method which is more advantageous in some of its features. The Pre-BiCG and Pre-BiCG-STAB methods are validated in terms of its efficiency and accuracy, by comparing with the contemporary iterative methods like Jacobi, GS and SOR. To calculate the benchmark

solutions we use spherical shell atmospheres. Few difficult test cases are also presented to show that the Pre-BiCG and Pre-BiCG-STAB are efficient numerical methods for spherical line transfer.

L. S. Anusha likes to thank Dr. Han Uitenbroek, Dr. A. Asensio Ramos and Dr. M. Sampurna for useful discussions.

REFERENCES

- Asensio Ramos, A., & Trujillo Bueno, J. 2006, in EAS Pub. Ser. 18, Radiative Transfer and Applications to Very Large Telescopes, ed. Ph. Stee, 25
- Auer, L. H. 1984, in Methods in radiative transfer, ed. Kalkofen, W. (Cambridge: Cambridge University Press), 237
- Auer, L. H. 1991, in Stellar Atmospheres: Beyond Classical Models, ed. Crivellari, L., Hubeny, I., & Hummer, D. G. (Dordrecht: Kluwer Academic Publishers), 9
- Auer, L. H., Fabiani Bendicho, P., & Trujillo Bueno, J. 1994, A&A, 292, 599
- Cannon, C. J. 1973, JQSRT, 13, 627
- Chandrasekhar, S. 1934, MNRAS, 94, 522
- Chevallier, L., Paletou, F., & Rutily, B. 2003, A&A, 411, 221
- Daniel, F., & Cernicharo, J. 2008, A&A, 488, 1237
- Gros, M., Crivellari, L., & Simonneau, E. 1997, ApJ, 489, 331
- Hamann, W-R. 1985, A&A, 145, 443
- Hamann, W-R. 2003, in ASP Conf. Ser. 288, Stellar Atmosphere Modeling, ed. Hubeny, I., Mihalas, D., & Werner, K. (San Francisco: ASP), 171
- Hestenes, M. R., & Stiefel, E. 1952, Journal of Research of the National Bureau of Standards, 49(6), 409
- Hubeny, I., & Burrows, A. 2007, ApJ, 659, 1458
- Hubeny, I. in ASP Conf. Ser. 288, Stellar Atmosphere Modeling, ed. Hubeny, I., Mihalas, D., & Werner, K. (San Francisco: ASP), 17

- Hummer, D. G., & Rybicki, G. B. 1971, MNRAS, 152, 1
- Klein, R. I., Castor, J. I., Greenbaum, A., Taylor, D., & Dykema, P. G. 1989, JQSRT, 41, 199
- Kosirev, N. A. 1934, MNRAS, 94, 430
- Kunasz, P. B., & Auer, L. H. 1988, JQSRT, 39, 67
- Kunasz, P. B., & Hummer, D. G. 1973, MNRAS, 166, 57
- Kunasz, P. B., & Hummer, D. G. 1974, MNRAS, 166, 19
- Mihalas, D. 1978, Stellar Atmospheres (2nd ed.; San Francisco: Freeman)
- Olson, G. L., Auer, L. H., & Buchler, J. R. 1986, JQSRT, 35, 431
- Paletou, F., & Anterrieu. 2009, arXiv:0905.3258, <http://arxiv.org/abs/0905.3258>
- Peraiah, A. 2002, An Introduction to Radiative Transfer (Cambridge University Press)
- Peraiah, A., & Grant, I. P. 1973, JIMA, 12, 75
- Saad, Y. 2000, Iterative methods for Sparse Linear Systems (2nd ed.)
- Scharmer, G. B. 1981, ApJ, 249, 720
- Schmid-Burgk, J. 1974, A&A, 32, 73
- Trujillo Bueno, J., & Fabiani Bendicho, P. 1995, ApJ, 455, 646
- Werner, K., & Husfeld, D. 1985, A&A, 148, 417

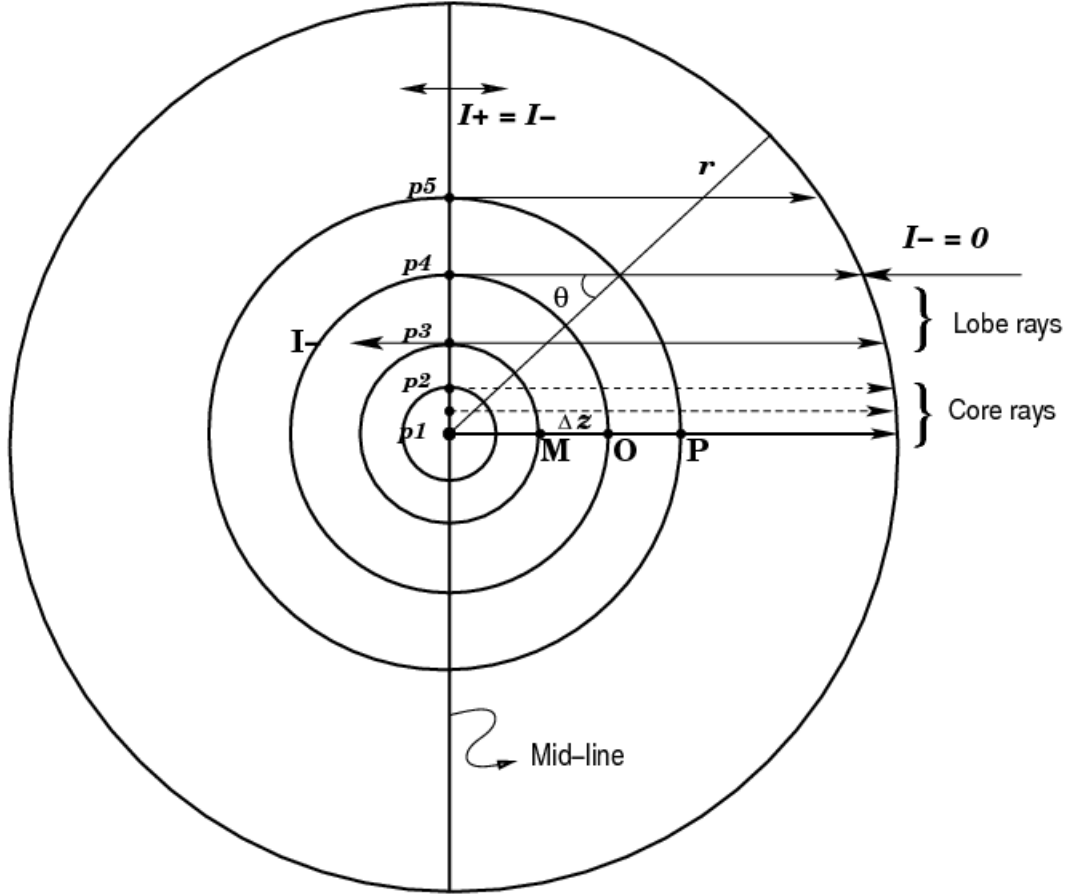


Fig. 1.— Geometry of the problem showing the computation of radiation field in a spherically symmetric system. The set of core rays and tangent rays are marked. The core is defined as a sphere with radius $r = 1$ in units of the core radius R_{core} . The surface is a sphere of radius $r = R$ in units of R_{core} . The rays that intersect the core are called ‘core rays’, and the rest are called ‘lobe rays’. No radiation is incident on the outer surface of the sphere (outer boundary condition). For all the examples presented in this paper, we use a reflecting boundary condition at the $z = 0$ vertical axis (the mid-line), namely same inner boundary conditions are used for both the core and the lobe rays.

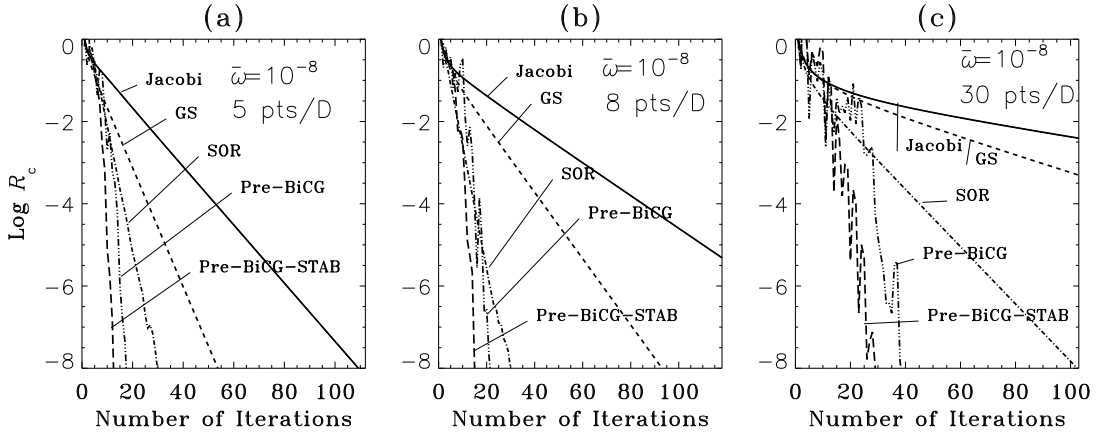


Fig. 2.— Dependence of the Maximum Relative Change R_c on the iterative progress for different methods. Panels (a), (b), and (c) represent models with low, medium and high spatial resolution respectively. The model parameters are $(\tilde{n}, R, T, a, \epsilon, \beta_c, B_\nu) = (0, 10, 10^3, 10^{-3}, 10^{-4}, 0, 1)$. The convergence criteria is chosen arbitrarily as $\bar{\omega} = 10^{-8}$. The SOR parameter $\omega = 1.5$. The figures show clearly that Jacobi method has the smallest convergence rate, which progressively increases for GS and SOR methods. Pre-BiCG and Pre-BiCG-STAB methods generally have the largest convergence rate compared to the other three.

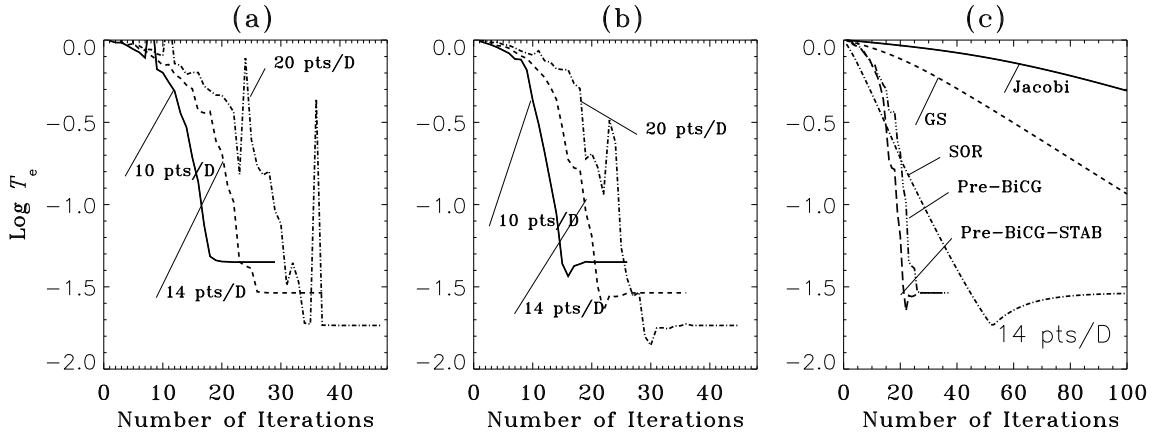


Fig. 3.— Behaviour of the true error T_e in a spherically symmetric medium. The model parameters are $(\tilde{n}, R, T, \epsilon, \beta_c, B_\nu) = (0, 10, 10^3, 10^{-4}, 0, 1)$. Panel (a) shows the decrement of the true error of the Pre-BiCG method for three different spatial grid resolutions. Notice the plateau in the true error. Panel (b) shows T_e for Pre-BiCG-STAB method. Panel (c) shows for different methods, the number of iterations required to reach a constant true error 2.9×10^{-2} . The SOR parameter $\omega = 1.5$. The overall behaviour of the curves is same for all the methods, although the rates of decrement are different.

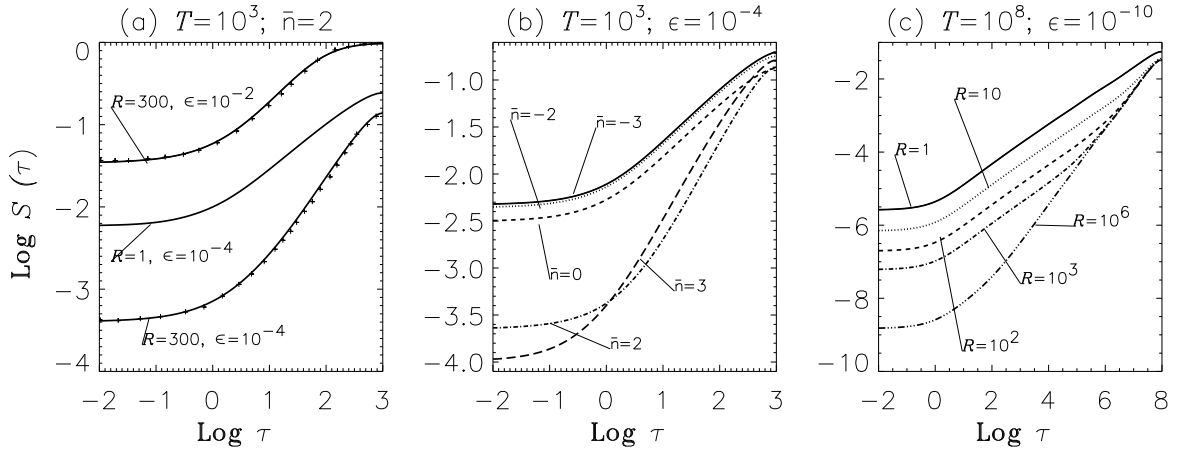


Fig. 4.— In panel (a) the source function variation with optical depth is shown for a spherical media with inverse square opacity variation for two different values of ϵ . The symbols show the benchmark solution read from Kunasz & Hummer (1974), which compare well with the solution by our method (Pre-BiCG - full lines). The plane parallel solution ($R = 1$) is shown for comparison. Panel (b) shows the effect of power law opacity indices \bar{n} on the source function variation with τ . In panel (c) the effects of spherical extension R are shown by taking a difficult case of highly scattering, effectively optically thin medium.

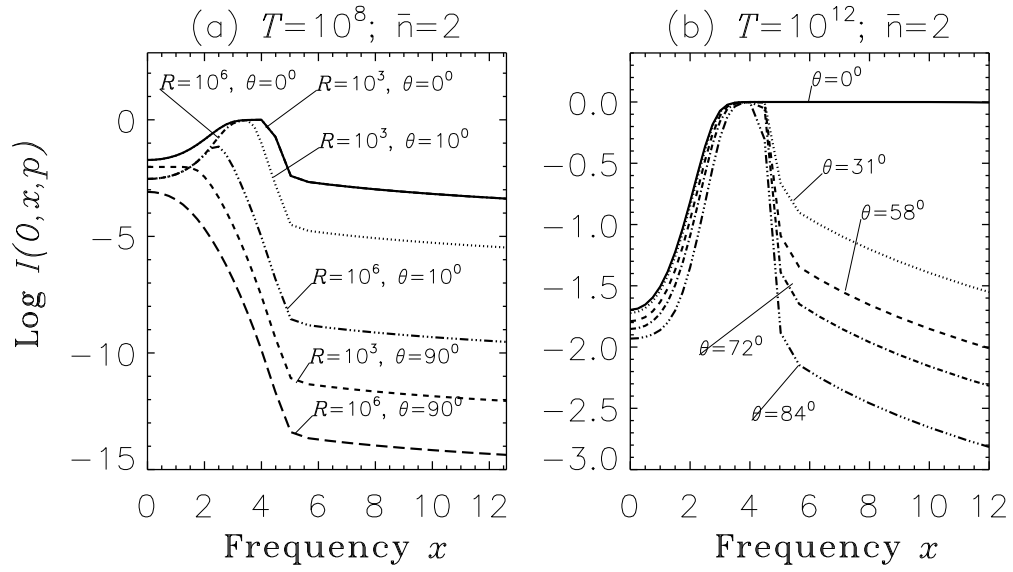


Fig. 5.— Angular dependence of emergent intensities in highly extended spherical media ($R = 10^3$ and $R = 10^6$). In panel (a) the profiles for the central ray ($\theta = 0^\circ$), and the lobe rays ($\theta = 10^\circ, 90^\circ$) are shown. Panel (b) shows the line profiles formed in a semi-infinite spherical atmosphere with $R = 300$ and $T = 10^{12}$.

Table 1: The sensitivity of different iterative methods to the convergence criteria $\bar{\omega}$. Tables 1(a), 1(b), 1(c) correspond respectively to $\bar{\omega}=10^{-6}$, 10^{-8} , and 10^{-10} . Number of points per decade in the logarithmic τ scale is denoted by $[N_{\text{pts}}/D]$. The SOR parameter used is 1.5. The entries under each method indicate the number of iterations required for convergence.

(a) $\bar{\omega}=10^{-6}$					
$[N_{\text{pts}}/D]$	Jacobi	GS	SOR	Pre-BiCG	Pre-BiCG-STAB
5	81	40	24	16	12
8	136	69	22	19	15
30	444	230	74	33	23
(b) $\bar{\omega}=10^{-8}$					
$[N_{\text{pts}}/D]$	Jacobi	GS	SOR	Pre-BiCG	Pre-BiCG-STAB
5	110	54	30	18	13
8	186	94	30	22	15
30	635	325	103	39	30
(c) $\bar{\omega}=10^{-10}$					
$[N_{\text{pts}}/D]$	Jacobi	GS	SOR	Pre-BiCG	Pre-BiCG-STAB
5	138	68	37	20	14
8	236	118	40	25	18
30	827	419	132	45	30

A. Construction of \hat{A} matrix and Preconditioner matrix \hat{M}

In Pre-BiCG method, it is essential to compute and store the \hat{A}^T matrix. A brute force - fully numerical way of doing this is as follows. Suppose that the dimension of \hat{A} matrix is $N_d \times N_d$, where N_d is the number of depth points. By sending a δ -source function N_d times, to a formal solver subroutine, N_d columns of \hat{A} matrix can be calculated. But this takes a large amount of CPU time especially for large values of N_d .

Instead, there is a semi-analytic way of calculating the \hat{A} matrix. By substituting the δ -source function in the expression for the intensity on a short-characteristic stencil of 3-points (MOP in standard notation) we can obtain “recursive relations for intensity matrix elements $\mathbf{I}_{ij}(i, j, = 1, 2, \dots N_d)$, which can then be integrated over frequencies and angles to get the $\hat{\Lambda}$ matrix. Finally, $\hat{A} = [\hat{I} - (1 - \epsilon)\hat{\Lambda}]$. The diagonal of $\hat{\Lambda}$ is $\hat{\Lambda}^*$ and the diagonal of \hat{A} is the preconditioner matrix \hat{M} .

For plane parallel full-slab problem, this is given in Kunasz & Auer (1988). In radiative transfer problems with spherical symmetry, it is sufficient to compute the solution on a quadrant. However this causes a tricky situation, in which we have to define a mid-line (see Fig. 1) on which a non-zero boundary condition $\mathbf{I}^+ = \mathbf{I}^-$ has to be specified. For the outgoing rays, the mid-vertical line is the starting grid point for a given ray. Since

Table 2: Timing efficiency of the iterative methods

	Jacobi	GS	SOR	Pre-BiCG	Pre-BiCG-STAB
CPU time for convergence	7 min 49 sec	4 min 4 sec	1 min 18 sec	27 sec	42 sec
Oerrates in computing	6 sec	6 sec	6 sec	9 sec	6 sec
Total computing time	7 min 55 sec	4 min 10 sec	1 min 24 sec	36 sec	48 sec

the intensity at the starting point is non-zero ($\mathbf{I}^+ = \mathbf{I}^-$), intensity at any interior point depends on the intensity at all the previous points. Recall that

$$\mathbf{I}_k(\mu > 0) = \mathbf{I}_{k+1}(\mu > 0) \exp(-\Delta\tau_k(\mu > 0)) + \Psi_{k-1}\mathbf{S}_{k-1} + \Psi_k\mathbf{S}_k + \Psi_{k+1}\mathbf{S}_{k+1} \quad (\text{A1})$$

and

$$\mathbf{I}_{k+1}(\mu > 0) = \mathbf{I}_{k+2}(\mu > 0) \exp(-\Delta\tau_{k+1}(\mu > 0)) + \Psi_k\mathbf{S}_k + \Psi_{k+1}\mathbf{S}_{k+1} + \Psi_{k+2}\mathbf{S}_{k+2} \quad (\text{A2})$$

and so on until we reach the mid-line. It is easy to see from above equations that intensity calculation at a short-characteristic stencil MOP is not confined only to the intensity on MOP, but also on all previous points, through spatial coupling. This is specific to performing radiative transfer on a spherical quadrant. Note that even for the construction of a diagonal $\hat{\Lambda}$, all the elements \mathbf{I}_{ij} of the intensity matrix has to be computed. We present below the recursive relations to compute $\mathbf{I}_{ij}(i, j = 1, 2, \dots, N_d)$.

For the incoming rays ($\mu < 0$) - Reverse sweep

DO $i = 1, 2, \dots, N_d$

Consider an arbitrary spatial point i . The delta-source vector is specified as

$$\mathbf{S}(\tau_i) = 1, \quad \mathbf{S}(\tau_j) = 0 \quad \text{for } i \neq j. \quad (\text{A3})$$

DO $ip = 1, 2, \dots, N_p$, where N_p is the total number of impact parameters.

For the inner boundary points, define $N_{v_p} = N_d$ for the core rays and $N_{v_p} = N_d - (ip - N_c - 1)$ for lobe rays. The index N_{v_p} represents the total number of points on a given ray of

constant impact parameter p . The external boundary condition has to be taken as zero for constructing integral operators like $\hat{\Lambda}$.

$$\mathbf{I}_{i1}(\tau_i, \tau_1, x, p) = 0. \quad (\text{A4})$$

For those rays (with index ip) for which $p(ip) \leq r(i)$

DO $j = 2, 3, \dots, N_{vp}$

IF

($j = i + 1$) and ($j = N_d$ or $p(ip) = r(j)$), which are interior boundary points

$$\mathbf{I}_{i,j}(\tau_i, \tau_j, x, p) = \mathbf{I}_{i,j-1}(\tau_i, \tau_{j-1}, x, p) \exp(-\Delta\tau_j(\mu)) + \Psi_u(j, x, p, \mu < 0) + \Psi_d(j, x, p, \mu < 0) \quad (\text{A5})$$

This is because at these interior boundary points we assume $\mathbf{S}_d = \mathbf{S}_u$ and $\mathbf{S}_d = \mathbf{S}_u = 1$ when $j = i + 1$.

ELSE

(Non interior boundary points)

If $j = i + 1$

$$\mathbf{I}_{i,j}(\tau_i, \tau_j, x, p) = \mathbf{I}_{i,j-1}(\tau_i, \tau_{j-1}, x, p) \exp(-\Delta\tau_j(\mu)) + \Psi_d(j, x, p, \mu < 0) \quad (\text{A6})$$

Elseif $j = i$

$$\mathbf{I}_{i,j}(\tau_i, \tau_j, x, p) = \mathbf{I}_{i,j-1}(\tau_i, \tau_{j-1}, x, p) \exp(-\Delta\tau_j(\mu)) + \Psi_0(j, x, p, \mu < 0) \quad (\text{A7})$$

Elseif $j = i - 1$

$$\mathbf{I}_{i,j}(\tau_i, \tau_j, x, p) = \mathbf{I}_{i,j-1}(\tau_i, \tau_{j-1}, x, p) \exp(-\Delta\tau_j(\mu)) + \Psi_u(j, x, p, \mu < 0) \quad (\text{A8})$$

Else

if ($j \leq i - 2$)

$$\mathbf{I}_{i,j}(\tau_i, \tau_j, x, p) = 0 \quad (\text{A9})$$

else

$$\mathbf{I}_{i,j}(\tau_i, \tau_j, x, p) = \mathbf{I}_{i,j-1}(\tau_i, \tau_{j-1}, x, p) \exp(-\Delta\tau_j(\mu)) \quad (\text{A10})$$

end if

End if

END IF

END DO

For those rays for which $p(ip) > r(i)$

DO $j = 2, 3, \dots, N_{vp}$

$$\mathbf{I}_{i,j}(\tau_i, \tau_j, x, p) = 0 \quad (\text{A11})$$

END DO

END DO

END DO

For the outgoing rays ($\mu > 0$) - Forward sweep

Let $i = N_d, N_d - 1, \dots, 1$

$$\mathbf{S}(\tau_i) = 1, \quad \mathbf{S}(\tau_j) = 0 \quad \text{for } i \neq j \quad (\text{A12})$$

DO $ip = 1, 2, \dots, N_p$

For $j = N_{vp}$ (Inner boundary point)

$$\mathbf{I}_{i,j}(\tau_i, \tau_j, x, p) \quad (\mu > 0) = \mathbf{I}_{i,j}(\tau_i, \tau_j, x, p) \quad (\mu < 0) \quad (\text{A13})$$

For non boundary points

For those rays (with index ip) for which $p(ip) \leq r(i)$

DO $j = N_{\text{vp}} - 1, N_{\text{vp}} - 2, \dots, 1$

If $j = i + 1$

$$\mathbf{I}_{i,j}(\tau_i, \tau_j, x, p) = \mathbf{I}_{i,j+1}(\tau_i, \tau_{j+1}, x, p) \exp(-\Delta\tau_j(\mu)) + \Psi_d(j, x, p, \mu > 0) \quad (\text{A14})$$

Elseif $j = i$

$$\mathbf{I}_{i,j}(\tau_i, \tau_j, x, p) = \mathbf{I}_{i,j+1}(\tau_i, \tau_{j+1}, x, p) \exp(-\Delta\tau_j(\mu)) + \Psi_0(j, x, p, \mu > 0) \quad (\text{A15})$$

Elseif $j = i - 1$

$$\mathbf{I}_{i,j}(\tau_i, \tau_j, x, p) = \mathbf{I}_{i,j+1}(\tau_i, \tau_{j+1}, x, p) \exp(-\Delta\tau_j(\mu)) + \Psi_u(j, x, p, \mu > 0) \quad (\text{A16})$$

Else

$$\mathbf{I}_{i,j}(\tau_i, \tau_j, x, p) = \mathbf{I}_{i,j+1}(\tau_i, \tau_{j+1}, x, p) \exp(-\Delta\tau_j(\mu)) \quad (\text{A17})$$

End if

END DO

For those rays for which $p(ip) > r(i)$

DO $j = N_{\text{vp}}, N_{\text{vp}} - 1, \dots, 1$

$$\mathbf{I}_{i,j}(\tau_i, \tau_j, x, p) = 0 \quad (\text{A18})$$

END DO

END DO

END DO

The algorithm given above saves a great deal of computing time by cutting down the number of calls to the formal solver -2 instead of N_d -the first call to store the Ψ and $\Delta\tau$ at all depth points, and the second call to compute \mathbf{I}_{ij}